Saudi Journal of Biological Sciences 28 (2021) 7517–7527

Contents lists available at ScienceDirect

Saudi Journal of Biological Sciences

journal homepage: www.sciencedirect.com

Original article

Identification of SARS-CoV-2 inhibitors from extracts of *Houttuynia cordata* Thunb.

Arun Bahadur Gurung [a,*], Mohammad Ajmal Ali [b], Joongku Lee [c], Mohammad Abul Farah [d], Khalid Mashay Al-Anazi [d], Fahad Al-Hemaid [b]

[a] Department of Basic Sciences and Social Sciences, North-Eastern Hill University, Shillong 793022, Meghalaya, India
[b] Department of Botany and Microbiology, College of Science, King Saud University, Riyadh 11451, Saudi Arabia
[c] Department of Environment and Forest Resources, Chungnam National University, 99 Daehak-ro, Yuseong-gu, Daejeon 34134, Republic of Korea
[d] Department of Zoology, College of Science, King Saud University, Riyadh 11451, Saudi Arabia

ARTICLE INFO

Article history:
Received 22 July 2021
Revised 23 August 2021
Accepted 29 August 2021
Available online 6 September 2021

Keyword:
Coronaviruses
Coronaviral RdRp
Houttuynia cordata
Bioactive compounds
Natural products
COVID-19
SARS-CoV-2
Virtual screening
Molecular docking
Molecular dynamics simulation

ABSTRACT

Houttuynia cordata Thunb., a perennial herb belonging to the Saururaceae family is a well-known ingredient of Traditional Chinese medicine (TCM) with several therapeutic properties. During the severe acute respiratory syndrome (SARS) outbreak in China, it was one of the approved ingredients in SARS preventative formulations and therefore, the plant may contain novel bioactive chemicals that can be used to suppress the replication of severe acute respiratory syndrome coronavirus 2 (SARS-CoV-2), a virus for which there are currently no effective drugs available. Like all RNA viruses, SARS-CoV-2 encode RNA-dependent RNA polymerase (RdRp) enzyme which aids viral gene transcription and replication. The present study is aimed at understanding the potential of bioactive compounds from *H. cordata* as inhibitors of the SARS-CoV-2 RdRp enzyme. We investigated the drug-likeness of the plant's active constituents, such as alkaloids, polyphenols, and flavonoids, as well as their binding affinity for the RdRp enzyme. Molecular docking experiments show that compounds **3** (1,2,3,4,5-pentamethoxy-dibenzo-quinolin-7-one), **14** (7-oxodehydroasimilobine), and **21** (1,2-dimethoxy-3-hydroxy-5-oxonoraporphine) have a high affinity for the drug target and that the complexes are maintained by hydrogen bonds with residues like Arg553, Cys622 and Asp623, as well as hydrophobic interactions with other residues. The lead compounds' complexes with the target enzyme remained stable throughout the molecular dynamics simulation. Analysis of molecular mechanics Poisson–Boltzmann surface area (MM-PBSA) and molecular mechanics generalized Born surface area (MM-GBSA) revealed the key residues contributing considerably to binding free energy. Thus, the findings reveal the potential of *H. cordata* bioactive compounds as anti-SARS-CoV-2 drug candidate molecules against the target enzyme.

1. Introduction

Houttuynia cordata Thunb. is a flowering and perennial herb native to China, Japan, Korea, and Southeast Asia. It is the single species in the genus Houttuynia, which belongs to the Saururaceae family. It thrives in wet, shaded hillside, roadside, and field ridges between 300 and 2600 m in elevation (Jiangang et al., 2013). *H. cordata* has a slender stem and heart-shaped leaves and bears greenish-yellow flowers. It grows up to an average height of 15–50 cm. When rubbed, it has a fishy odour and a somewhat astringent flavour. When the stalk and leaves have matured, it is generally harvested in the summer or autumn (Yang and Jiang, 2009). In Southeast Asia's indigenous medicine systems, *H. cordata* is a well-known traditional medicinal ingredient (Jiangang et al., 2013). It relieves fever, resolves toxins, reduces edema, drains pus, and promotes urination (Zheng et al., 1998). It was one of the components in SARS preventive formulations authorized by the Chinese Ministry of Health during the epidemic of Severe Acute Respiratory Syndrome (SARS) (Lau et al., 2008). *H. cordata* has been utilized in China as an edible vegetable and an effective traditional Chinese medicine (TCM) since ancient times (Yang and Jiang, 2009). It has antileukemic (Kwon et al., 2003), antimutagenic

* Corresponding author.
E-mail address: arunbgurung@gmail.com (A. Bahadur Gurung).
Peer review under responsibility of King Saud University.

Production and hosting by Elsevier

https://doi.org/10.1016/j.sjbs.2021.08.100
1319-562X/

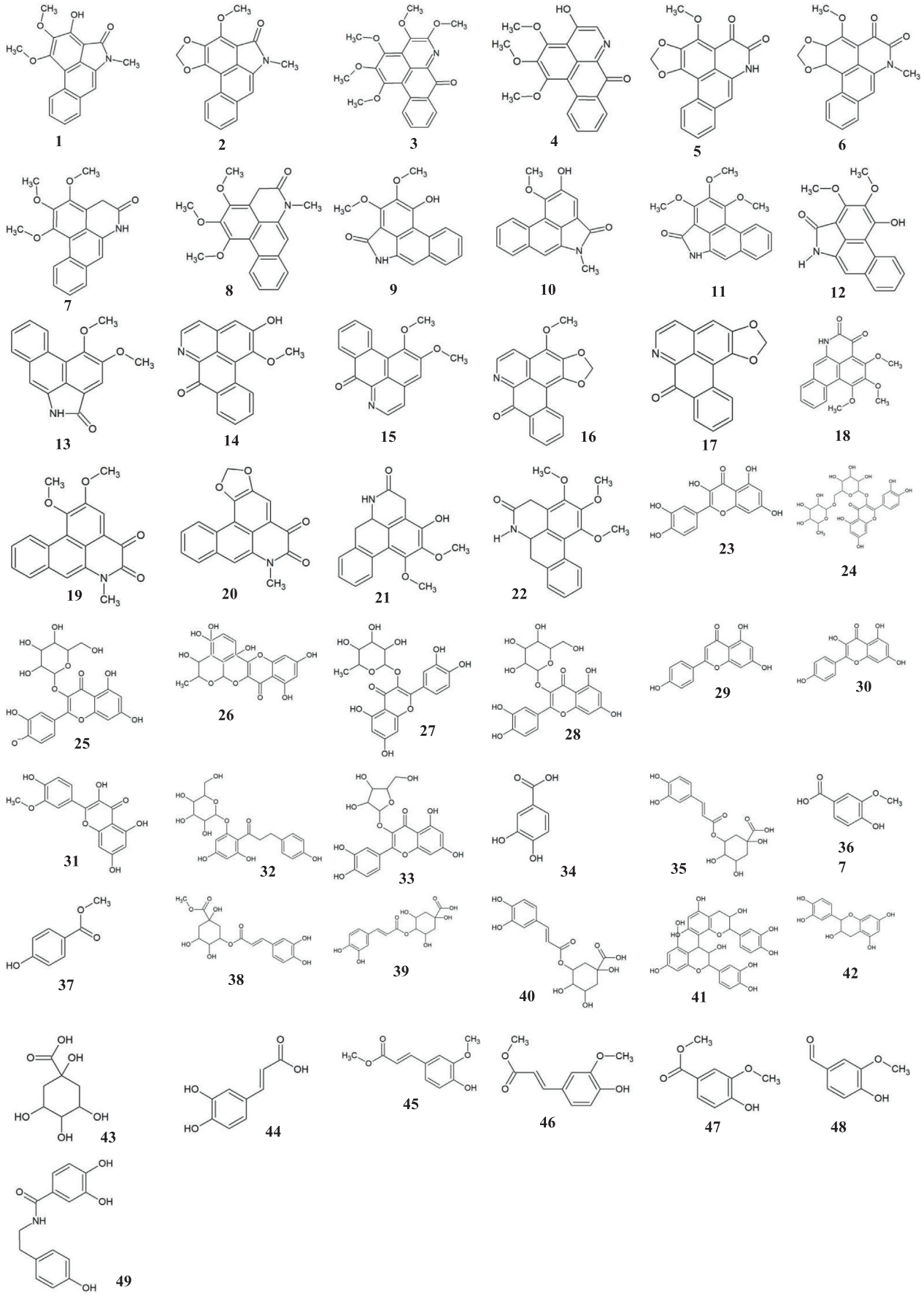

Fig. 1. Selected compounds belonging to different classes- alkaloids (**1**–**22**), flavonoids (**23**–**33**) and polyphenols (**34**–**49**) isolated from extracts of *H. cordata* used for virtual screening.

(Chen et al., 2003), anti-inflammatory (Chiang et al., 2003), and antianaphylaxis (Li et al., 2005) properties, as well as the potential to boost immunologic function. Amino acids, vitamins, and trace elements such as potassium, zinc, iron, copper, and manganese are the nutrients present in *H. cordata*. The active components in the plant include volatile oils, organic acids, flavonoids, alkaloids, polyphenols, water-soluble polysaccharides etc (Yang and Jiang, 2009).

Severe acute respiratory syndrome coronavirus 2 (SARS-CoV-2) is a highly transmissible and pathogenic coronavirus that first appeared in late 2019 and has since caused a pandemic of an acute respiratory disease known as coronavirus disease 2019 (COVID-19), which poses a threat to human health and public safety (Hu et al., 2021). SARS-CoV-2 is a new betacoronavirus with a genomic sequence that is 79 % similar to severe acute respiratory syndrome coronavirus (SARS-CoV) and 50 % similar to Middle East respiratory syndrome coronavirus (MERS-CoV) (Lu et al., 2020). SARS-CoV-2 is a positive-strand RNA virus with a genome of around 30 kb which encode 14 open reading frames (ORFs) (Jiang et al., 2021). All RNA viruses encode RNA-dependent RNA polymerases (RdRps) enzyme which aids viral gene transcription and replication in collaboration with other viral and host components (Gorbalenya et al., 2002). The RdRps are multi-domain proteins that catalyze the formation of phosphodiester linkages

Table 1
The list of bioactive molecules from *H. cordata* extract with their physicochemical characteristics. (* indicates the molecules that have favourable drug-like properties).

Compounds	Name	CID	MW[1]	LogP[2]	HBA[3]	HBD[4]	Mutagenic	Tumorigenic	Reproductive Effective	Irritant
1*	Piperolactam D homologue	–	301.341	2.6158	5	2	none	none	none	none
2	Analogue of compound 1	–	307.304	3.5685	5	0	high	high	none	high
3*	1,2,3,4,5-pentamethoxy-dibenzo-quinolin-7-one	–	381.383	3.4248	7	0	none	none	none	none
4*	4-hydroxy-1,2,3-trimethoxy-7H-dibenzo-quinolin-7-one	–	337.33	2.8677	6	1	none	none	none	none
5	3-methoxy-6H-benzodioxolo-benzoquinoline-4,5-dione	–	321.287	2.6483	6	1	high	high	none	high
6	3-methoxy-6-methyl-6H-benzodioxolo-benzoquinoline-4,5-dione	–	335.314	3.0066	6	0	high	high	none	high
7	1,2,3-trimethoxy-4H,6H-dibenzoquinolin-5-one	–	323.347	2.9477	5	1	high	high	none	high
8	1,2,3- trimethoxy-6-methyl-4H,6H-dibenzoquinolin-5-one	–	337.374	3.306	5	0	high	high	none	high
9	Piperolactam D	14,039,008	295.293	2.6831	5	2	high	high	none	high
10	Sauristolactam	131,002	279.294	3.1114	4	1	high	high	none	high
11	Piperolactam C	10,881,419	309.32	2.9588	5	1	high	high	none	high
12*	Piperolactam B	–	287.314	2.2643	5	2	none	none	none	none
13	Cepharanone B	162,739	279.294	3.0288	4	1	high	high	none	high
14*	7-oxodehydroasimilobine	–	277.278	3.0077	4	1	none	none	none	none
15*	Lysicamine	122,691	291.305	3.2834	4	0	none	none	none	none
16*	Atherospermidine	77,514	305.288	3.4648	5	0	none	none	none	none
17*	Liriodenine	10,144	275.262	3.5348	4	0	none	none	none	none
18	Ouregidione	11,958,181	337.33	2.3969	6	1	high	high	none	high
19	Cepharadione B	189,151	321.331	2.8252	5	0	high	high	none	high
20	Cepharadione A	94,577	305.288	3.0766	5	0	high	high	none	high
21*	1,2-dimethoxy-3-hydroxy-5-oxonoraporphine	–	311.336	2.3148	5	2	none	none	none	none
22*	1,2,3-trimethoxy-3-hydroxy-5-oxonoraporphine	–	325.363	2.5905	5	1	none	none	none	none
23	Quercetin	5,280,343	302.237	1.4902	7	5	high	high	none	none
24	Rutin	5,280,805	610.519	−1.2573	16	10	none	none	none	none
25	Hyperin	90,657,624	464.378	−0.3469	12	8	none	none	none	none
26	Afzelin	5,316,673	432.38	0.9255	10	6	none	none	none	none
27	Quercitrin	5,280,459	448.379	0.5798	11	7	none	none	none	none
28	Isoquercitrin	5,280,804	464.378	−0.3469	12	8	none	none	none	none
29	Apigenin	5,280,443	270.239	2.3357	5	3	high	none	none	none
30	Kaempferol	5,280,863	286.238	1.8359	6	4	high	none	none	none
31	Isorhamnetin	5,281,654	316.264	1.7659	7	4	high	none	none	none
32	Phloridzin	6072	436.412	0.055	10	7	none	none	low	none
33	Avicularin	5,490,064	434.352	0.1632	11	7	none	none	none	none
34	Protocatechuic acid	72	154.121	0.4533	4	3	high	none	none	none
35	Chlorogenic acid	1,794,427	354.31	−0.7685	9	6	none	none	none	none
36	Vanillic acid	8468	168.148	0.729	4	2	high	none	none	none
37*	*p*-Hydroxy-benzoic acid methyl ester	7456	152.149	1.2269	3	1	none	none	none	none
38*	Chlorogenic acid methyl ester	6,476,139	368.337	−0.3406	9	5	none	none	none	none
39	Cryptochlorogenic acid	9,798,666	354.31	−0.7685	9	6	none	none	none	none
40	Neochlorogenic acid	5,280,633	354.31	−0.7685	9	6	none	none	none	none
41	Procyanidin B	122,738	578.524	2.3016	12	10	none	none	high	none
42*	Catechin	73,160	290.27	1.5087	6	5	none	none	none	none
43*	Quinic acid	6508	192.166	−2.3347	6	5	none	none	none	none
44	Caffeic acid	689,043	180.159	0.7825	4	3	high	high	high	none
45*	*cis*-Methyl ferulate	10,176,654	208.212	1.4861	4	1	none	none	none	none
46*	*trans*-Methyl ferulate	5,357,283	208.212	1.4861	4	1	none	none	none	none
47*	Methyl vanillate	19,844	182.174	1.1569	4	1	none	none	none	none
48	Vanillin	1183	152.149	1.1772	3	1	high	none	high	high
49*	Houttuynamide A	44,521,377	273.287	1.9095	5	4	none	none	none	none

1: Molecular weight in g/mol; 2: Partition coefficient between *n*-octanol and water; 3: Hydrogen bond acceptor; 4: Hydrogen bond donor

Table 2
The inhibition constants and binding energies of selected compounds generated from *H.cordata* docked against the target enzyme. BE: Estimated Free Energy of Binding [BE = Final Intermolecular Energy + Final Total Internal Energy + Torsional Free Energy- Unbound System's Energy], where Final Intermolecular Energy = vdW + Hbond + desolv Energy + Electrostatic Energy; K_i: Estimated Inhibition Constant [Temperature = 298.15 K].

Molecules	Name	RdRp	
		BE (kcal/mol)	K_i (μM)
1	Piperolactam D homologue	−4.88	266.86
3	1,2,3,4,5-pentamethoxy-dibenzo-quinolin-7-one	−6.24	26.88
4	4-hydroxy-1,2,3-trimethoxy-7H-dibenzo-quinolin-7-one	−5.76	60.06
12	Piperolactam B	−5.62	75.76
14	7-oxodehydroasimilobine	−6.38	21.14
15	Lysicamine	−5.85	51.12
16	Atherospermidine	−6.06	36.06
17	Liriodenine	−6.05	36.50
21	1,2-dimethoxy-3-hydroxy-5-oxonoraporphine	−6.15	31.31
22	1,2,3-trimethoxy-3-hydroxy-5-oxonoraporphine	−5.84	52.66
37	*p*-Hydroxy-benzoic acid methyl ester	−4.69	363.94
38	Chlorogenic acid methyl ester	−5.98	41.10
42	Catechin	−5.61	76.81
43	Quinic acid	−4.79	308.10
45	*cis*-Methyl ferulate	−4.76	324.33
46	*trans*-Methyl ferulate	−4.66	381.50
47	Methyl vanillate	−4.14	916.44
49	Houttuynamide A	−5.41	107.56
Control	Remdesivir	−5.98	41.10

between ribonucleotides in the presence of a divalent metal ion using an RNA template (Jia and Gong, 2019). SARS-CoV-2 RdRp (also known as nsp12) is an important element of the replication/-transcription machinery (Pachetti et al., 2020). Nidovirus RdRp-associated nucleotidyltransferase (NiRAN) domain, interface domain, and C-terminal RdRp domain are all found in the nsp12 subunit (Gao et al., 2020). The RdRp domain, which is present in all single-subunit polymerases, is shaped like a right hand, with fingers, palm, and thumb subdomains (Kirchdoerfer and Ward, 2019). RdRp is one of the most important targets for antiviral medication research, as it is found in a wide range of viruses (Pachetti et al., 2020). Favipiravir (Furuta et al., 2013), Galidesivir (Lim et al., 2017), Remdesivir (Agostini et al., 2018), and Ribavirin (Morgenstern et al., 2005) are several RdRp inhibitors that have been proposed to target SARS-CoV-2.

The absence of effective treatments for human coronaviral infections (Jean et al., 2020), as well as the high fatality rates associated with the novel coronavirus (2019-nCoV) (Piroth et al., 2021), has prompted the development of new vaccines. In this study, we looked at the possibilities of utilizing *H. cordata* bioactive molecules to halt SARS-CoV-2 replication. We screened out drug-like molecules from *H. cordata* using *in silico* toxicity filters and utilized molecular docking and molecular dynamics to describe the binding interaction of the chosen bioactive compounds with the target enzyme (SARS-CoV-2 RdRp).

2. Materials and methods

2.1. Retrieval and preparation of bioactive alkaloids

The information on the various bioactive compounds of *H. cordata* was obtained from a literature search (Jiangang et al., 2013; Ma et al., 2017). A total of 49 molecules consisting of 22 alkaloids, 11 flavonoids and 16 polyphenols were chosen for the study. The 3D structures of the molecules were retrieved from the PubChem database (Kim et al., 2016) and the molecules whose three-dimensional structures were not available in the chemical databases were sketched using ACD/ChemSketch (Freeware) 2019.1.2 software and were processed into 3D structures using Open Babel version 2.4.1 software (O'Boyle et al., 2011) and further energy-optimized using Merck molecular force field (MMFF94) (Halgren, 1996) following our previously described protocol (Gurung et al., 2016). The molecules were prepared for docking using AutoDock Toos-1.5.6 by the addition of Gasteiger charges and hydrogen atoms and torsions for each molecule were optimally defined.

2.2. Virtual screening of drug-like molecules

The bioactive molecules were screened based on various drug-like filters such as Lipinski's rule of five parameters (Lipinski, 2004): molecular weight (MW) (<=500), hydrogen bond acceptor (HBA) (<=10), hydrogen bond donor (HBD) (<=5), partition coefficient between *n*-octanol and water (clogP) (<=5) and *in silico* toxicity filters such as mutagenicity, irritancy, tumourigenicity, reproductive health etc. DataWarrior program version 5.0 software (Sander et al., 2015) was used to analyze the physico-chemical characteristics of the selected compounds, such as drug-like properties and toxicity.

2.3. Retrieval and preparation of structure of drug target

The three-dimensional cryo-electron microscopy structure of the enzyme target-SARS-CoV-2 RdRp (PDB ID: 7BV2) at a resolution of 2.50 Å, was retrieved from Protein Data Bank (http://www.rcsb.org/). This crystal structure contains a ternary complex of RdRp enzyme (nsp12) with cofactors nsp7 and nsp8 bound to the template-primer RNA and triphosphate form of remdesivir (Yin et al., 2020). The target enzyme (nsp12) was prepared by deleting the cofactors and removing the heteroatoms including ions, co-crystallized ligands and water molecules. Further, an optimum number of polar hydrogen atoms and Kolmann charges were added to the target enzyme using AutoDock Toos-1.5.6.

2.4. Evaluation of binding affinity of the compounds with the target enzyme

The binding affinity of each molecule along with the control inhibitor was evaluated against the enzyme target using a molecular docking approach. The binding sites for the compounds were defined by choosing a grid box of dimensions of 60 × 60 × 60 $Å^3$ with a grid spacing value of 0.375 Å centred at x:92.5053, y:93.2594, z:103.4061 around the bound co-crystallized ligand. AutoDock 4.2 (Morris et al., 2009) was used for performing molecular docking study using Lamarckian genetic algorithm with fifty independent docking runs for each molecule including the cocrystal ligand (triphosphate form of remdesivir).

2.5. Evaluation of binding poses and molecular interactions

The binding poses for each molecule was considered based on the lowest binding energy score. LigPlot + tool version v.1.4.5 was used to analyse the molecular interactions (hydrogen bonds and hydrophobic interactions) between the target enzyme and compounds (Laskowski and Swindells, 2011).

2.6. Molecular dynamics simulation

The AMBER16 software, which is accessible on ligand and receptor molecular dynamics (LARMD) (http://chemyang.ccnu.edu.cn/ccb/server/LARMD/), was used to simulate the protein–ligand complexes for a 4-ns MD simulation in an explicit water

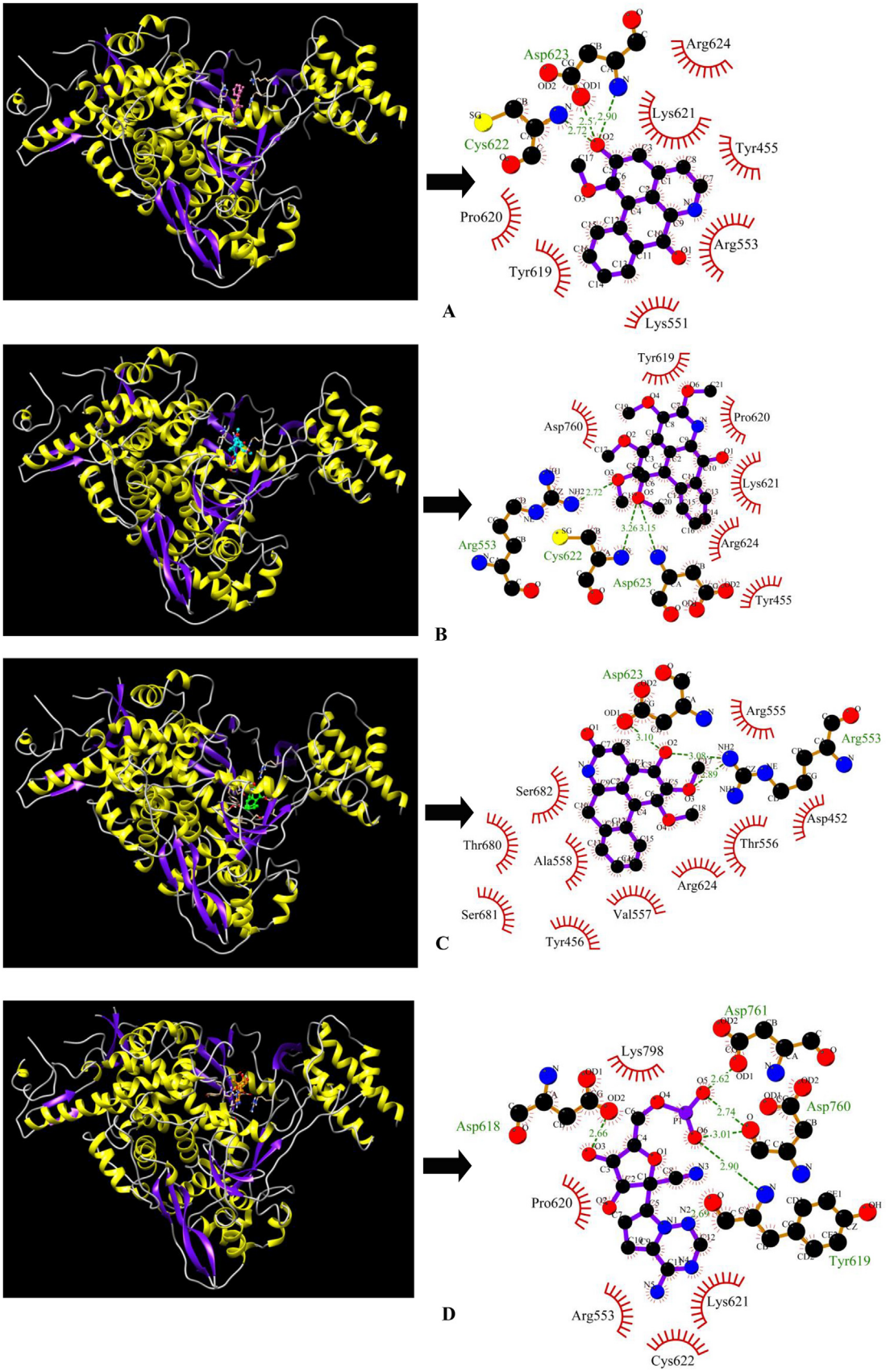

Fig. 2. Best docked molecules with the target enzyme-(A) RdRp_**14** (B) RdRp_**3** (C) RdRp_**21** (D) RdRp_remdesivir. Green dashed lines with the bond distance represent hydrogen bonds, whereas red arcs with spikes denote residues that contribute to hydrophobic interactions.

model (Yang et al., 2020). The following equation (1) was used to determine the binding free energy (ΔG_{bind})

$$\Delta G_{bind} = \Delta E_{bind} - T\Delta S_{sol} - T\Delta S_{con} \quad (1)$$

where ΔE_{bind} is the binding energy, $T\Delta S_{sol}$ is the solvation entropy, and $T\Delta S_{conf}$ is the conformational entropy. The entropy was estimated using the MM/PB (GB) SA technique (Hou et al., 2011), and the enthalpy was computed using an empirical approach (Hao et al., 2009; Pan et al., 2008).

3. Results

A total of 49 major bioactive molecules as shown in Fig. 1 comprising of 22 alkaloids, 11 flavonoids and 16 polyphenols were subjected to virtual screening based on Lipinski's rule of five and *in silico* toxicity filters such as mutagenicity, irritancy, tumourigenicity and reproductive health. Out of 49 bioactive molecules, 18 molecules (10 alkaloids and 8 polyphenols) successfully passed the drug-like filters (the rule of five and toxicity filters) (Table 1). The binding affinities of these drug-like bioactive molecules were evaluated against the target enzyme-SARS-CoV-2 RdRp using molecular docking. The docking scores of the molecules were compared with the control inhibitor Remdesivir which is bound as a co-crystal structure. The top three lead molecules identified for SARS-CoV-2 RdRp were 7-oxodehydroasimilobine (**14**), 1,2,3,4,5-pentamethoxy-dibenzo-quinolin-7-one (**3**) and 1,2-dimethoxy-3-hydroxy-5-oxonoraporphine (**21**) with binding energies of −6.38 kcal/mol, −6.24 kcal/mol and −6.15 kcal/mol respectively and their corresponding inhibition constants were 21.14 μM, 26.88 μM and 31.31 μM (Table 2). The best lead molecule **14** binds to RdRp enzyme through three hydrogen bonds- one with backbone nitrogen (N) atom of Asp623, one with side chain OD1 atom of Asp623 and one with backbone nitrogen (N) atom of Cys622 and the binding pose further shows the participation of seven residues (Tyr455, Lys551, Arg553, Tyr619, Pro620, Lys621 and Arg624) in hydrophobic interactions with SARS-CoV-2 RdRp (Fig. 2**A**). The second lead molecule **3** binds to RdRp enzyme through three hydrogen bonds-one with backbone nitrogen (N) atom of Asp623, the second one with backbone nitrogen (N) atom of Cys622 and the third one with the side chain nitrogen (NH2) atom of Arg553 and hydrophobic interactions through six residues (Tyr455, Tyr619, Pro620, Lys621, Arg624 and Asp760) (Fig. 2**B**). The third lead molecule **21** binds to the RdRp enzyme through three hydrogen bonds-one with the side chain oxygen (OD1) atom of Asp623, two hydrogen bonds with the side chain nitrogen (NH2) atom of Arg553 and hydrophobic interactions through ten residues (Asp452, Tyr456, Arg555, Thr556, Val557, Ala558, Arg624, Thr680, Ser681 and Ser682) (Fig. 2C). The control inhibitor Remdesivir shows binding energy of −5.78 kcal/mol and inhibition constant of 41.10 μM with six hydrogen bonds-one with the side chain oxygen (OD2) atom of Asp618, the second one with the side chain oxygen (OD1) atom of Asp761, the third and the fourth one with the backbone oxygen (O) atom of Asp760, the fifth one with the backbone nitrogen (N) atom of Tyr619 and the sixth one with the backbone oxygen (O) atom of Tyr619 and hydrophobic interactions via residues- Arg553, Pro620, Lys621, Cys622 and Lys798 (Fig. 2**D**).

Molecular dynamics simulations in an aqueous environment with a simulation period of 4 ns were used to investigate the stability of the best-docked molecules with the RdRp enzyme. The root mean square deviation (RMSD), radius of gyration (Rg), and percentage of native contacts (Q) values of the protein–ligand complexes were computed to determine the system's stability. The RMSD estimates the measurement of root mean square deviation of atomic positions which is used to determine the average distance between the atoms of superimposed structures of protein and ligand over a period of time (Maiorov and Crippen, 1994). The average RMSD of Cα atoms of RdRp and heavy atoms of **14** in RdRp_**14** complex was found to be 1.491471829 ± 0.22338225 4 Å and 0.227194732 ± 0.085059128 Å respectively (Fig. 3**a**). Whereas, RdRp_**3** complex has an average RMSD of 1.508672829 ± 0.250546445 Å for Cα atoms of RdRp and 0.545165463 ± 0.13 4428523 Å for heavy atoms of **3** (Fig. 3**b**). The average RMSD of Cα atoms of RdRp and heavy atoms of **21** in RdRp_**21** complex

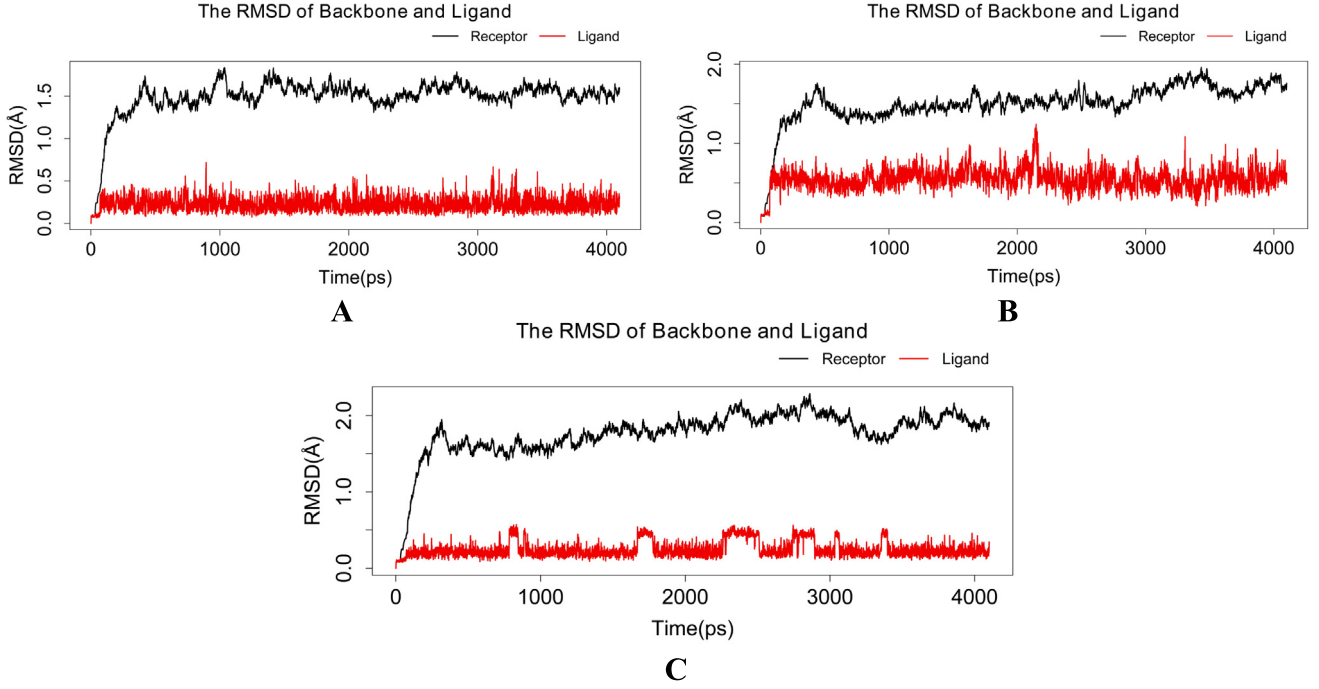

Fig. 3. Plot of root mean square deviation (RMSD) versus time (ps) for (a) RdRp_**14** (b) RdRp_**3** (c) RdRp_**21.** The black line represents the RMSD curve of protein backbone atoms, whereas the red line represents the RMSD curve of ligand heavy atoms.

was found to be 1.769013366 ± 0.305136961 Å and 0.245875439 ± 0.105217219 Å respectively with respect to the starting structures (Fig. 3**c**). Rg can be explained as the root mean square distance from each atom of the system to its centre of mass (Lobanov et al., 2008). The Rg values for protein–ligand complexes: RdRp_**14**, RdRp_**3** and RdRp_**21** show stable fluctuation between 28.8 and 29.2 Å, 28.6 to 29.2 Å and 28.7 to 29.1 respectively (Fig. 4**)**. With a folding free energy barrier, the Q (fraction of native contacts) represents conformational dynamics and transition states of a protein (Best et al., 2013). The Q values RdRp_**14**, RdRp_**3** and RdRp_**21** were found to be 0.963516973 ± 0.010784 854, 0.970136286 ± 0.009314162 and 0.961349858 ± 0.01155158 1 respectively (Fig. 5). Essential dynamics (ED) or Principal component analysis is a reliable approach for grouping protein conformations and distinguishing large concerted patterns of fluctuations from MD simulation trajectories (Gurung et al., 2021). The contribution of eigenvector 1 (PC1) towards the total mean square fluctuations were found to be 140.626 $Å^2$ (19.051%), 200.317 $Å^2$ (24.243%) and 225.722 $Å^2$ (25.526%) for RdRp_**14**, RdRp_**3** and RdRp_**21** respectively (Fig. 6). Eigenvector 2 contributions to the total mean square fluctuations RdRp_**14**, RdRp_**3** and RdRp_**21** were calculated to be 78.101 $Å^2$ (10.581%), 118.850 $Å^2$ (14.384%) and 121.656 $Å^2$ (13.758%), 81.949 $Å^2$ respectively. Whereas eigenvector 3 (PC3) also shares significant contributions to the total mean square fluctuations in RdRp_**14**, RdRp_**3** and RdRp_**21** complexes with their corresponding eigenvalues as 66.559 $Å^2$ (9.017%), 52.241 $Å^2$ (6.322%) and 54.767 $Å^2$ (6.193%).

The binding free energies between RdRp and **14** (ΔPB = -3.75 k cal/mol, ΔGB = -5.02 kcal/mol), **3** (ΔPB = 11.80 kcal/mol, ΔGB = 10. 99 kcal/mol) and **21** (ΔPB = -7.71 kcal/mol, ΔGB = -11.95 kcal/mol) were calculated using Molecular mechanics Poisson–Boltzmann surface area (MM-PBSA) and molecular mechanics generalized

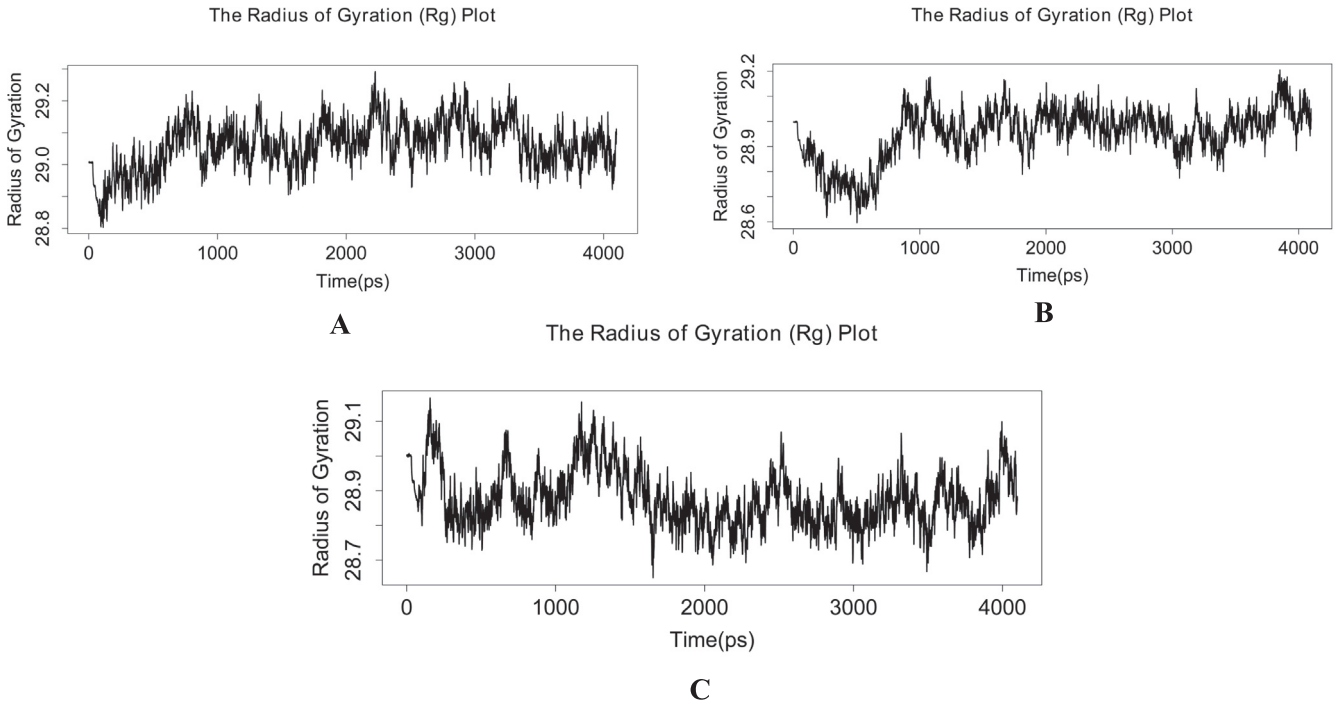

Fig. 4. Plot of radius of gyration (Rg) versus time (ps) for (a) RdRp_**14** (b) RdRp_**3** (c) RdRp_**21.**

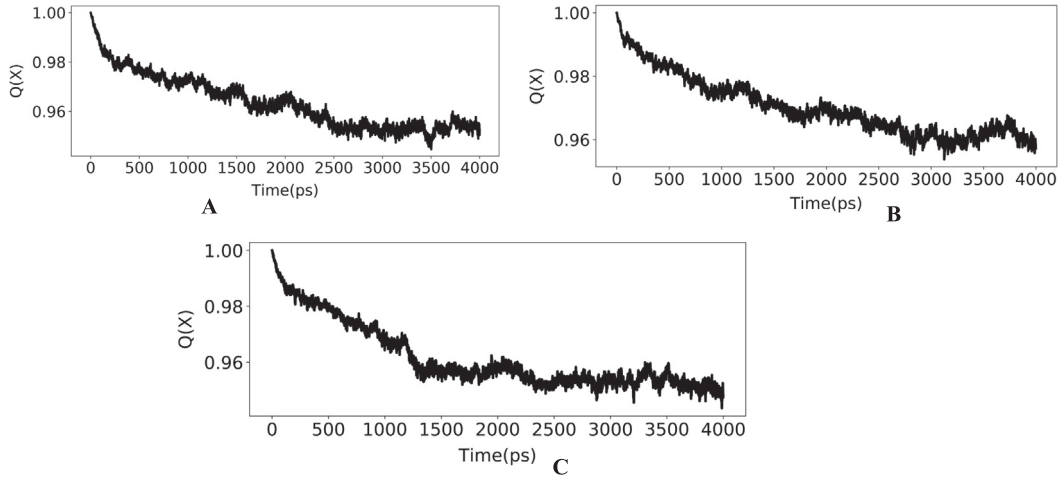

Fig. 5. Plot of native contacts (Q) versus time (ps) for (a) RdRp_**14** (b) RdRp_**3** (c) RdRp_**21.**

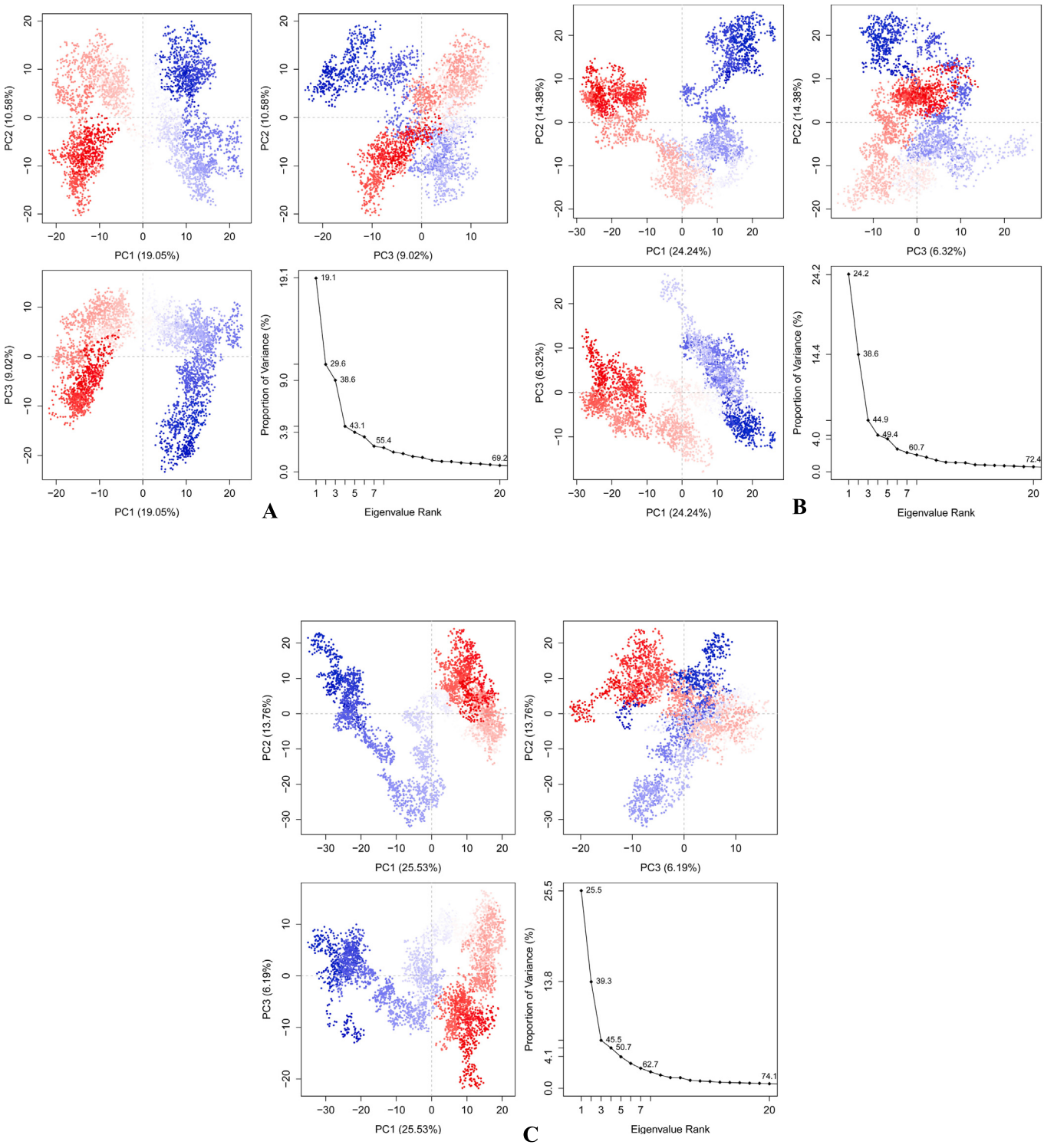

Fig. 6. Principal component analysis (PCA) for (a) RdRp_**14** (b) RdRp_**3** (c) RdRp_**21.**

Born surface area (MM-GBSA) methods. (Table 3). In all the three protein–ligand complexes except RdRp_**3**, the major contribution to the binding energy is by the van der Waals energy component. The top ten residues contributing towards the binding interaction between RdRp and **14** include Asp452, Tyr455, Ser549, Lys551, Arg553, Pro620, Lys621, Cys622, Asp623 and Arg624 (Fig. 7**a**). The residues such as Tyr455, Lys551, Arg553, Asp618, Tyr619, Lys621, Asp623, Asp760, Asp761 and Lys798 contribute significantly to the total binding energy between RdRp and **3** (Fig. 7**b**). Similarly, the top ten residues contributing towards the binding interaction between RdRp and **21** include Asp452, Tyr455, Arg553, Thr556, Val557, Asp623, Arg624, Ser681, Ser682 and Thr687 (Fig. 7**c**).

4. Discussion

Medicinal plants have long been recognized as a source of therapeutics, and they continue to be a valuable resource for discover-

Table 3
Summary of the binding free energy of protein–ligand complexes (in kcal/mol).

Protein-ligand complexes	ELE[1]	VDW[2]	GAS[3]	PBSOL[4]	PBTOT[5]	GBSOL[4]	GBTOT[5]	-TS[6]	$\triangle G^{7}_{PB}$	$\triangle G^{7}_{GB}$
RdRp_**14**	−3.37 ± 2.49	−25.62 ± 2.11	−28.99 ± 3.55	11.07 ± 3.93	−17.92 ± 2.75	9.80 ± 2.43	−19.19 ± 1.79	14.17 ± 1.94	−3.75	−5.02
RdRp_**3**	−48.71 ± 11.17	−25.82 ± 3.77	−74.53 ± 12.36	65.94 ± 11.97	−8.59 ± 4.81	65.13 ± 10.48	−9.40 ± 3.27	20.39 ± 3.48	11.80	10.99
RdRp_**21**	−8.40 ± 1.99	−30.20 ± 2.94	−38.60 ± 3.95	17.56 ± 3.17	−21.04 ± 3.02	13.32 ± 1.77	−25.28 ± 2.99	13.33 ± 1.93	−7.71	−11.95

[1]Electrostatic energy as calculated by the MM force field; [2]Van der Waals contribution from MM; [3]Total gas-phase energy; [4]Non-polar and polar contributions to solvation based on PB/GB model; [5]Final estimated binding free energy calculated from GAS and PBSOL/GBSOL; [6]Entropy; [7]Binding free energy with entropy

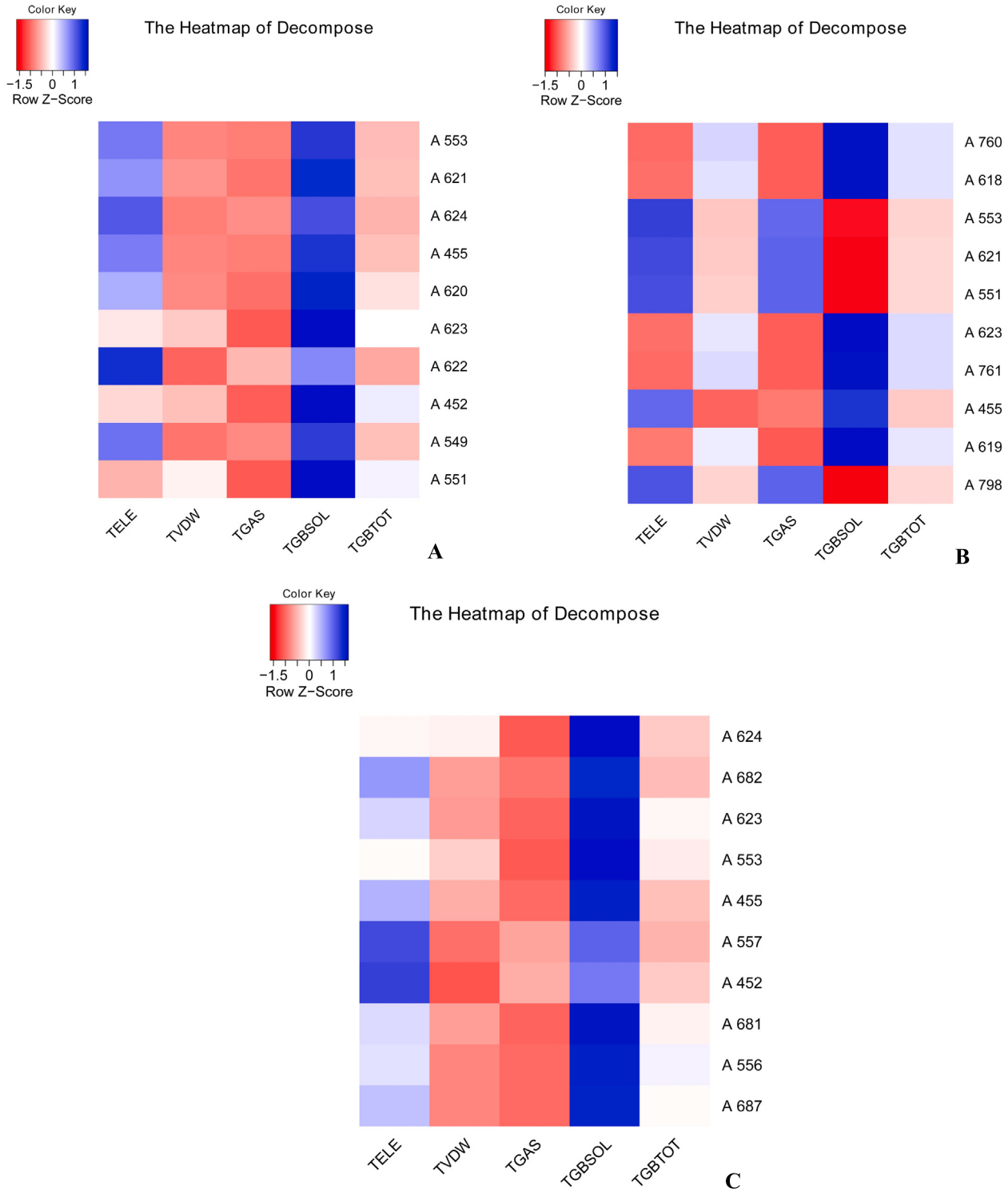

Fig. 7. The decomposition of binding free energy for the top ten residues depicted in a heatmap for (a) RdRp_**14** (b) RdRp_**3** (c) RdRp_**21.**

ing new drug candidates (Atanasov et al., 2015). Many of these plants have been used in traditional medicine to treat diseases that are viral in origin (Ben-Shabat et al., 2020). Besides gaining a better understanding of pathological processes, the pharmaceutical industry has been concerned about the source of molecules. Natural medicines are gaining popularity due to several advantages, including lower costs, acceptability due to a long history of usage, better patient tolerance, and fewer or no adverse effects (Akram et al., 2018). In the present study, we explored the potential of three major classes of phytochemicals-alkaloids, flavonoids and polyphenols from *H. cordata* as inhibitors of the SARS-CoV-2 RdRp enzyme. *H. cordata* (Saururaceae) is a traditional Chinese medicine (TCM) that has been used for hundreds of years to treat pulmonary-related problems such as abscesses, phlegm, cough, and dyspnea and is effective in the treatment of pneumonia, infectious disease, and other respiratory disorders (Lau et al., 2008). Besides, the plant has anti-inflammatory (Park et al., 2005), anti-allergic (Kim et al., 2007), virucidal (Chiang et al., 2003), anti-oxidative (Ng et al., 2007), and anti-cancer properties (Kim et al., 2001). RdRp, one of the most important drug targets found in several viruses is a major component of the SARS-CoV-2 replication/-transcription machinery (Pachetti et al., 2020). In our present studies, compounds **14** (7-oxodehydroasimilobine), **3** (1,2,3,4,5-pentamethoxy-dibenzo-quinolin-7-one) and **21** (1,2-dimethoxy-3-hydroxy-5-oxonoraporphine) were found to be the most potent bioactive molecules interacting with the enzyme target with a binding affinity higher than the control (remdesivir). The complexes of these lead molecules with the target enzyme remained stable throughout the simulation time in terms of the root mean square deviation (RMSD), radius of gyration (Rg), and percentage of native contacts (Q) plots. Remdesivir, an adenosine analogue first designed for hepatitis C and later investigated for Ebola is a competitive inhibitor of RdRp enzyme (Triggle et al., 2021). All the three best-docked molecules of *H. cordata* in our studies belong to the alkaloids class. Alkaloids are a class of natural compounds produced from plants that have potent antiviral properties and therefore, represent potential candidates for finding effective COVID-19 therapies (Majnooni et al., 2021). Compound **14** had substantial protein tyrosine phosphatase 1B (PTP1B) inhibitory action with an IC50 value of 2.672 μM while **3** (10 μM) had modest hepatoprotective efficacy against D-galactosamine-induced WB-F344 cell injury (Ma et al., 2017). PTP1B is a validated therapeutic target for type 2 diabetes since it acts as a negative regulator of insulin signalling pathways (Shrestha et al., 2019). Previous studies investigating the immunological and antiviral aspects of SARS-preventive mechanisms of *H. cordata* found that the HC water extract stimulates significant proliferation of mouse splenic lymphocytes, increased the proportion of CD4 + and CD8 + T cells, and a significant increase in the secretion of IL-2 and IL-10, and exhibited significant antiviral properties by inhibiting SARS-CoV RdRp and 3C-like protease ($3CL^{pro}$) enzymes (Lau et al., 2008). Further, the anti-SARS-CoV-2 potential of *H. cordata* was recently demonstrated by Das et al. (2021) whose studies suggested 6-Hydroxyondansetron and Quercitrin as a new therapeutic drug against COVID-19. Both these compounds showed good binding with three SARS-CoV-2 protein receptors such as main protease (M^{pro}), papain-like protease (PL^{pro}) and ADP-ribose phosphatase (ADRP).

5. Conclusion

The binding of drug-like bioactive compounds of *H. cordata* to the RdRp, an enzyme involved in the replication and transcription of SARS-CoV-2, was investigated using molecular modelling techniques such as molecular docking and dynamics simulation. Compounds **14** (7-oxodehydroasimilobine), **3** (1,2,3,4,5-pentamethoxy-dibenzo-quinolin-7-one) and **21** (1,2-dimethoxy-3-hydroxy-5-oxo noraporphine) were found to be best docked to the target enzyme and formed stable protein–ligand complexes throughout the simulation time. These compounds may be developed into promising drug candidates for SARS-CoV-2 infections.

Declaration of Competing Interest

The authors declare that they have no known competing financial interests or personal relationships that could have appeared to influence the work reported in this paper.

Acknowledgements

The authors would like to extend their sincere appreciation to the Researchers Supporting Project number (RSP-2021/306), King Saud University, Riyadh, Saudi Arabia.

References

Agostini, M.L., Andres, E.L., Sims, A.C., Graham, R.L., Sheahan, T.P., Lu, X., Smith, E.C., Case, J.B., Feng, J.Y., Jordan, R., Ray, A.S., Cihlar, T., Siegel, D., Mackman, R.L., Clarke, M.O., Baric, R.S., Denison, M.R., Subbarao, K., Gallagher, T., Enjuanes, L., 2018. Coronavirus susceptibility to the antiviral remdesivir (GS-5734) is mediated by the viral polymerase and the proofreading exoribonuclease. MBio 9 (2). https://doi.org/10.1128/mBio.00221-18.

Akram, M., Tahir, I.M., Shah, S.M.A., Mahmood, Z., Altaf, A., Ahmad, K., Munir, N., Daniyal, M., Nasir, S., Mehboob, H., 2018. Antiviral potential of medicinal plants against HIV, HSV, influenza, hepatitis, and coxsackievirus: a systematic review. Phyther. Res. 32 (5), 811–822.

Atanasov, A.G., Waltenberger, B., Pferschy-Wenzig, E.-M., Linder, T., Wawrosch, C., Uhrin, P., Temml, V., Wang, L., Schwaiger, S., Heiss, E.H., Rollinger, J.M., Schuster, D., Breuss, J.M., Bochkov, V., Mihovilovic, M.D., Kopp, B., Bauer, R., Dirsch, V.M., Stuppner, H., 2015. Discovery and resupply of pharmacologically active plant-derived natural products: A review. Biotechnol. Adv. 33 (8), 1582–1614.

Ben-Shabat, S., Yarmolinsky, L., Porat, D., Dahan, A., 2020. Antiviral effect of phytochemicals from medicinal plants: applications and drug delivery strategies. Drug Deliv. Transl. Res. 10 (2), 354–367.

Best, R.B., Hummer, G., Eaton, W.A., 2013. Native contacts determine protein folding mechanisms in atomistic simulations. Proc. Natl. Acad. Sci. 110 (44), 17874–17879.

CHEN, Y.-Y., LIU, T.-F., CHEN, C.-M., CHAO, P.-Y., CHANG, T.-J., 2003. A study of the antioxidative and antimutagenic effects of Houttuynia cordata Thunb. using an oxidized frying oil-fed model. J. Nutr. Sci. Vitaminol. (Tokyo) 49 (5), 327–333.

Chiang, L.-C., Chang, J.-S., Chen, C.-C., Ng, L.-T., Lin, C.-C., 2003. Anti-Herpes simplex virus activity of Bidens pilosa and Houttuynia cordata. Am. J. Chin. Med. 31 (03), 355–362.

Das, S.K., Mahanta, S., Tanti, B., Tag, H., Hui, P.K., 2021. Identification of phytocompounds from Houttuynia cordata Thunb. as potential inhibitors for SARS-CoV-2 replication proteins through GC–MS/LC–MS characterization, molecular docking and molecular dynamics simulation. Mol. Divers, 1–24.

Furuta, Y., Gowen, B.B., Takahashi, K., Shiraki, K., Smee, D.F., Barnard, D.L., 2013. Favipiravir (T-705), a novel viral RNA polymerase inhibitor. Antiviral Res. 100 (2), 446–454.

Gao, Y., Yan, L., Huang, Y., Liu, F., Zhao, Y., Cao, L., Wang, T., Sun, Q., Ming, Z., Zhang, L., Ge, J.i., Zheng, L., Zhang, Y., Wang, H., Zhu, Y., Zhu, C., Hu, T., Hua, T., Zhang, B., Yang, X., Li, J., Yang, H., Liu, Z., Xu, W., Guddat, L.W., Wang, Q., Lou, Z., Rao, Z., 2020. Structure of the RNA-dependent RNA polymerase from COVID-19 virus. Science (80-.) 368 (6492), 779–782.

Gorbalenya, A.E., Pringle, F.M., Zeddam, J.-L., Luke, B.T., Cameron, C.E., Kalmakoff, J., Hanzlik, T.N., Gordon, K.H.J., Ward, V.K., 2002. The palm subdomain-based active site is internally permuted in viral RNA-dependent RNA polymerases of an ancient lineage. J. Mol. Biol. 324 (1), 47–62.

Gurung, A.B., Ali, M.A., Lee, J., Farah, M.A., Al-Anazi, K.M., 2021. Identification of potential SARS-CoV-2 entry inhibitors by targeting the interface region between the spike RBD and human ACE2. J. Infect. Public Health 14 (2), 227–237.

Gurung, A.B., Bhattacharjee, A., Ali, M.A., 2016. Exploring the physicochemical profile and the binding patterns of selected novel anticancer Himalayan plant derived active compounds with macromolecular targets. Informatics Med. Unlocked 5, 1–14.

Halgren, T.A., 1996. Merck molecular force field. I. Basis, form, scope, parameterization, and performance of MMFF94. J. Comput. Chem. 17, 490–519. https://doi.org/10.1002/(SICI)1096-987X(199604)17:5/6<490::AID-JCC1>3.0.CO;2-P.

Hao, G.-F., Zhu, X.-L., Ji, F.-Q., Zhang, L.i., Yang, G.-F., Zhan, C.-G., 2009. Understanding the mechanism of drug resistance due to a codon deletion in protoporphyrinogen oxidase through computational modeling. J. Phys. Chem. B 113 (14), 4865–4875.

Hou, T., Wang, J., Li, Y., Wang, W., 2011. Assessing the performance of the MM/PBSA and MM/GBSA methods. 1. The accuracy of binding free energy calculations based on molecular dynamics simulations. J. Chem. Inf. Model. 51 (1), 69–82.
Hu, B., Guo, H., Zhou, P., Shi, Z.-L., 2021. Characteristics of SARS-CoV-2 and COVID-19. Nat. Rev. Microbiol. 19 (3), 141–154.
Jean, S.-S., Lee, P.-I., Hsueh, P.-R., 2020. Treatment options for COVID-19: The reality and challenges. J. Microbiol. Immunol. Infect. 53 (3), 436–443.
Jia, H., Gong, P., 2019. A structure-function diversity survey of the RNA-dependent RNA polymerases from the positive-strand RNA viruses. Front. Microbiol. 10, 1945.
Jiang, Y.i., Yin, W., Xu, H.E., 2021. RNA-dependent RNA polymerase: Structure, mechanism, and drug discovery for COVID-19. Biochem. Biophys. Res. Commun. 538, 47–53.
Jiangang, F., Ling, D., Zhang, L., Hongmei, L., 2013. Houttuynia cordata Thunb: a review of phytochemistry and pharmacology and quality control. Chin Med. 2013.
Kim, I.S., Kim, J.-H., Kim, J.S., Yun, C.-Y., Kim, D.-H., Lee, J.-S., 2007. The inhibitory effect of Houttuynia cordata extract on stem cell factor-induced HMC-1 cell migration. J. Ethnopharmacol. 112 (1), 90–95.
Kim, S.-K., Ryu, S.Y., No, J., Choi, S.U., Kim, Y.S., 2001. Cytotoxic alkaloids from Houttuynia cordate. Arch. Pharm. Res. 24 (6), 518–521.
Kim, S., Thiessen, P.A., Bolton, E.E., Chen, J., Fu, G., Gindulyte, A., Han, L., He, J., He, S., Shoemaker, B.A., Wang, J., Yu, B.o., Zhang, J., Bryant, S.H., 2016. PubChem Substance and Compound databases. Nucleic Acids Res 44 (D1), D1202–D1213. https://doi.org/10.1093/nar/gkv951.
Kirchdoerfer, R.N., Ward, A.B., 2019. Structure of the SARS-CoV nsp12 polymerase bound to nsp7 and nsp8 co-factors. Nat. Commun. 10, 1–9.
Kwon, K.-B., Kim, E.-K., Shin, B.-C., Seo, E.-A., Yang, J.-Y., Ryu, D.-G., 2003. Herba houttuyniae extract induces apoptotic death of human promyelocytic leukemia cells via caspase activation accompanied by dissipation of mitochondrial membrane potential and cytochrome c release. Exp. Mol. Med. 35 (2), 91–97.
Laskowski, R.A., Swindells, M.B., 2011. LigPlot+: multiple ligand-protein interaction diagrams for drug discovery. J. Chem. Inf. Model. 51 (10), 2778–2786. https://doi.org/10.1021/ci200227u.
Lau, K.-M., Lee, K.-M., Koon, C.-M., Cheung, C.-F., Lau, C.-P., Ho, H.-M., Lee, M.-H., Au, S.-N., Cheng, C.-K., Lau, C.-S., Tsui, S.-W., Wan, D.-C., Waye, M.-Y., Wong, K.-B., Wong, C.-K., Lam, C.-K., Leung, P.-C., Fung, K.-P., 2008. Immunomodulatory and anti-SARS activities of Houttuynia cordata. J. Ethnopharmacol. 118 (1), 79–85.
Li, G.Z., Chai, O.H., Lee, M.S., Han, E.-H., Kim, H.T., Song, C.H., 2005. Inhibitory effects of Houttuynia cordata water extracts on anaphylactic reaction and mast cell activation. Biol. Pharm. Bull. 28 (10), 1864–1868.
Lim, S.-Y., Osuna, C., Lakritz, J., Chen, E., Yoon, G., Taylor, R., MacLennan, S., Leonard, M., Giuliano, E., Mathis, A., others, 2017. Galidesivir, a direct-acting antiviral drug, Abrogates Viremia in Rhesus Macaques challenged with zika virus, in: Open Forum Infectious Diseases.
Lipinski, C.A., 2004. Lead- and drug-like compounds: the rule-of-five revolution. Drug Discov. Today. Technol. 1, 337–341. https://doi.org/10.1016/j.ddtec.2004.11.007.
Lobanov, M.Y., Bogatyreva, N.S., Galzitskaya, O.V., 2008. Radius of gyration as an indicator of protein structure compactness. Mol. Biol. 42, 623–628.
Lu, R., Zhao, X., Li, J., Niu, P., Yang, B.o., Wu, H., Wang, W., Song, H., Huang, B., Zhu, N. a., Bi, Y., Ma, X., Zhan, F., Wang, L., Hu, T., Zhou, H., Hu, Z., Zhou, W., Zhao, L.i., Chen, J., Meng, Y., Wang, J.i., Lin, Y., Yuan, J., Xie, Z., Ma, J., Liu, W.J., Wang, D., Xu, W., Holmes, E.C., Gao, G.F., Wu, G., Chen, W., Shi, W., Tan, W., 2020. Genomic characterisation and epidemiology of 2019 novel coronavirus: implications for virus origins and receptor binding. Lancet 395 (10224), 565–574.
Ma, Q., Wei, R., Wang, Z., Liu, W., Sang, Z., Li, Y., Huang, H., 2017. Bioactive alkaloids from the aerial parts of Houttuynia cordata. J. Ethnopharmacol. 195, 166–172.
Maiorov, V.N., Crippen, G.M., 1994. Significance of root-mean-square deviation in comparing three-dimensional structures of globular proteins.
Majnooni, M.B., Fakhri, S., Bahrami, G., Naseri, M., Farzaei, M.H., Echeverria, J., 2021. Alkaloids as Potential Phytochemicals against SARS-CoV-2: Approaches to the Associated Pivotal Mechanisms. Evidence-Based Complement. Altern. Med.
Morgenstern, B., Michaelis, M., Baer, P.C., Doerr, H.W., Cinatl Jr, J., 2005. Ribavirin and interferon-β synergistically inhibit SARS-associated coronavirus replication in animal and human cell lines. Biochem. Biophys. Res. Commun. 326, 905–908.
Morris, G.M., Huey, R., Lindstrom, W., Sanner, M.F., Belew, R.K., Goodsell, D.S., Olson, A.J., 2009. AutoDock4 and AutoDockTools4: Automated docking with selective receptor flexibility. J. Comput. Chem. 30 (16), 2785–2791. https://doi.org/10.1002/jcc.v30:1610.1002/jcc.21256.
Ng, L.-T., Yen, F.-L., Liao, C.-W., Lin, C.-C., 2007. Protective effect of Houttuynia cordata extract on bleomycin-induced pulmonary fibrosis in rats. Am. J. Chin. Med. 35 (03), 465–475.
O'Boyle, N.M., Banck, M., James, C.A., Morley, C., Vandermeersch, T., Hutchison, G.R., 2011. Open Babel: An open chemical toolbox. J. Cheminform. 3, 33. https://doi.org/10.1186/1758-2946-3-33.
Pachetti, M., Marini, B., Benedetti, F., Giudici, F., Mauro, E., Storici, P., Masciovecchio, C., Angeletti, S., Ciccozzi, M., Gallo, R.C., Zella, D., Ippodrino, R., 2020. Emerging SARS-CoV-2 mutation hot spots include a novel RNA-dependent-RNA polymerase variant. J. Transl. Med. 18 (1). https://doi.org/10.1186/s12967-020-02344-6.
Pan, Y., Gao, D., Zhan, C.-G., 2008. Modeling the catalysis of anti-cocaine catalytic antibody: competing reaction pathways and free energy barriers. J. Am. Chem. Soc. 130 (15), 5140–5149.
Park, E., Kum, S., Wang, C., Park, S.Y., Kim, B.S., Schuller-Levis, G., 2005. Anti-inflammatory activity of herbal medicines: inhibition of nitric oxide production and tumor necrosis factor-$α$ secretion in an activated macrophage-like cell line. Am. J. Chin. Med. 33 (03), 415–424.
Piroth, L., Cottenet, J., Mariet, A.-S., Bonniaud, P., Blot, M., Tubert-Bitter, P., Quantin, C., 2021. Comparison of the characteristics, morbidity, and mortality of COVID-19 and seasonal influenza: a nationwide, population-based retrospective cohort study. Lancet Respir. Med. 9 (3), 251–259.
Sander, T., Freyss, J., von Korff, M., Rufener, C., 2015. DataWarrior: an open-source program for chemistry aware data visualization and analysis. J. Chem. Inf. Model. 55 (2), 460–473. https://doi.org/10.1021/ci500588j.
Shrestha, S., Seong, S.H., Park, S.G., Min, B.S., Jung, H.A., Choi, J.S., 2019. Insight into the PTP1B inhibitory activity of arylbenzofurans: An in vitro and in silico study. Molecules 24 (16), 2893. https://doi.org/10.3390/molecules24162893.
Triggle, C.R., Bansal, D., Ding, H., Islam, M.M., Farag, E.A.B.A., Hadi, H.A., Sultan, A.A., 2021. A comprehensive review of viral characteristics, transmission, pathophysiology, immune response, and management of SARS-CoV-2 and COVID-19 as a basis for controlling the pandemic. Front. Immunol. 12, 338.
Yang, J.-F., Wang, F., Chen, Y.-Z., Hao, G.-F., Yang, G.-F., 2020. LARMD: integration of bioinformatic resources to profile ligand-driven protein dynamics with a case on the activation of estrogen receptor. Brief. Bioinform. 21, 2206–2218.
Yang, L.i., Jiang, J.-G., 2009. Bioactive components and functional properties of Hottuynia cordata and its applications. Pharm. Biol. 47 (12), 1154–1161.
Yin, W., Mao, C., Luan, X., Shen, D.-D., Shen, Q., Su, H., Wang, X., Zhou, F., Zhao, W., Gao, M., et al., 2020. Structural basis for inhibition of the RNA-dependent RNA polymerase from SARS-CoV-2 by remdesivir. Science (80-.).
Zheng, H.Z., Dong, Z.H., She, J., 1998. Modern study of traditional Chinese medicine. Xue Yuan Press Beijing China 3, 2057.